ADVANCED FUNCTIONAL MATERIALS
www.afm-journal.de

Check for updates

Nanocellulose-Carboxymethylcellulose Electrolyte for Stable, High-Rate Zinc-Ion Batteries

*Lin Xu, Taotao Meng, Xueying Zheng, Tangyuan Li, Alexandra H. Brozena, Yimin Mao, Qian Zhang, Bryson Callie Clifford, Jiancun Rao, and Liangbing Hu**

Aqueous Zn ion batteries (ZIBs) are one of the most promising battery chemistries for grid-scale renewable energy storage. However, their application is limited by issues such as Zn dendrite formation and undesirable side reactions that can occur in the presence of excess free water molecules and ions. In this study, a nanocellulose-carboxymethylcellulose (CMC) hydrogel electrolyte is demonstrated that features stable cycling performance and high Zn^{2+} conductivity (26 mS cm^{-1}), which is attributed to the material's strong mechanical strength (≈70 MPa) and water-bonding ability. With this electrolyte, the Zn-metal anode shows exceptional cycling stability at an ultra-high rate, with the ability to sustain a current density as high as 80 mA cm^{-2} for more than 3500 cycles and a cumulative capacity of 17.6 Ah cm^{-2} (40 mA cm^{-2}). Additionally, side reactions, such as hydrogen evolution and surface passivation, are substantially reduced due to the strong water-bonding capacity of the CMC. Full Zn||MnO_2 batteries fabricated with this electrolyte demonstrate excellent high-rate performance and long-term cycling stability (>500 cycles at 8C). These results suggest the cellulose-CMC electrolyte as a promising low-cost, easy-to-fabricate, and sustainable aqueous-based electrolyte for ZIBs with excellent electrochemical performance that can help pave the way toward grid-scale energy storage for renewable energy sources.

1. Introduction

Battery technology will play a pivotal role in the effort toward decarbonization and the fight against global warming by more fully enabling the use of renewable energy sources.[1–3] Aqueous Zn ion batteries (ZIBs) are one of the most promising battery chemistries for applications such as grid-scale energy storage as they are safer than flammable organic-based systems, low-cost, environmentally friendly, and feature rapid charge/discharge rates.[4–7] However, despite these advantages, ZIBs have not been widely commercialized, largely due to undesirable interactions between the electrolyte and Zn-metal anode, including dendritic growth on the anode surface, side reactions forming an inert passivation layer, as well as hydrogen evolution during the plating/stripping process.[8–14] These effects can cause poor cycling reversibility of the Zn-metal anode, leading to battery failure on the anode side.

Many strategies of electrolyte modification have been explored to promote reversible Zn plating. While water is necessary in aqueous Zn ion batteries for ionic conduction, reducing the free water content in the electrolyte helps eliminate detrimental side reactions. Methods based on this approach include "water-in-salt" electrolytes that feature ultra-high salt concentrations[15–17] or the use of additives that act as water blockers.[18,19] However, such liquid electrolytes do not provide additional mechanical strength to prevent dendritic growth and are therefore unable to sustain high current densities. To address this issue, hydrogel electrolytes have been developed, which feature a denser structure that helps inhibit the growth of Zn dendrites. Cellulose, which is one of the most abundant biomaterials on earth and is inherently a low-cost, green material,[20,21] has been studied extensively as a key building block of such hydrogel electrolytes for aqueous Zn ion batteries.[22–37] In addition to providing mechanical strength that helps prevent dendrite growth, the cellulose structure helps to bond water and therefore limit the free water content to decrease interfacial side reactions.[38,39] However, the molecular structure of cellulose limits how much water it can bond. As a result, cellulose-based electrolytes often feature either too much free water, which causes parasitic side reactions, or too little water after drying intended to remove free water, which leads to low Zn conductivities (**Figure 1**A). Additionally, many cellulose-based hydrogel electrolytes incorporate multiple, synthetic cross-linking additives (e.g., polyacrylamide) to

L. Xu, T. Meng, X. Zheng, T. Li, A. H. Brozena, Y. Mao, Q. Zhang, B. C. Clifford, L. Hu
Department of Materials Science and Engineering
University of Maryland
College Park, MD 20742, USA
E-mail: binghu@umd.edu
J. Rao
Advanced Imaging and Microscopy Laboratory
University of Maryland
College Park, MD 20742, USA
The ORCID identification number(s) for the author(s) of this article can be found under https://doi.org/10.1002/adfm.202302098.

© 2023 The Authors. Advanced Functional Materials published by Wiley-VCH GmbH. This is an open access article under the terms of the Creative Commons Attribution License, which permits use, distribution and reproduction in any medium, provided the original work is properly cited.

DOI: 10.1002/adfm.202302098

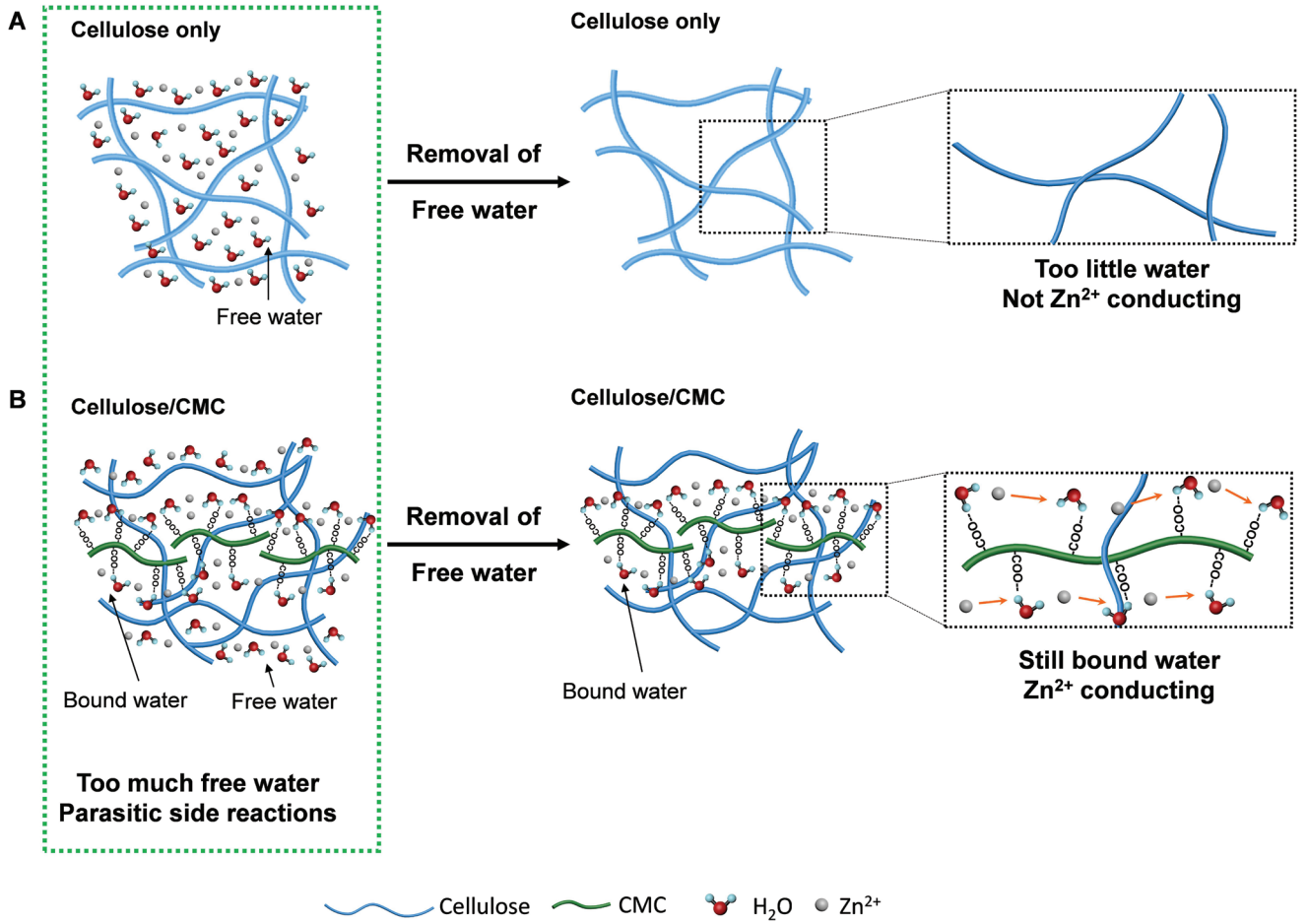

Figure 1. Cellulose-CMC electrolyte for aqueous Zn ion batteries. A) When the electrolyte membrane is made of pure cellulose, there is either too much free water that causes parasitic side reactions, or too little water after drying that causes low Zn^{2+} conductivity. B) In contrast, by adding CMC within the cellulose matrix, after a squeeze-dry process to reduce the amount of free water molecules and to mitigate parasitic side reactions, there are still water molecules bonded along the CMC chains, which enables the transport of the Zn ions.

increase the mechanical strength of the membrane. But this approach limits the biodegradability of the material and increases the cost of processing. As a result, it has remained challenging to develop an electrolyte for aqueous ZIBs that enables high stability, cyclability, and the capability to withstand high current densities for high power density energy storage.

In this work, we demonstrate a nanocellulose-carboxymethylcellulose (CMC) electrolyte that features high ionic conductivity, mechanical strength, and low free water content that enables both high-rate and long-cycle-life aqueous ZIBs. In this approach, CMC polymer chains are distributed within the relatively ridged cellulose network (Figure 1B) to form a dense, quasi-solid-state electrolyte that also functions as the battery separator. CMC, an inexpensive and commercially available cellulose derivative, features numerous carboxyl groups that form stronger bonding interactions with water molecules compared to cellulose alone,[40,41] which can help limit the free water content when used in a membrane. The increased bound water content helps promote Zn ion conductivity, while simultaneously preventing excess free water molecules from engaging in parasitic side reactions. Additionally, a facile NaOH treatment increases the tensile strength of the cellulose-CMC electrolyte to >70 MPa. As a result, the cellulose-CMC electrolyte shows a high Zn ionic conductivity of up to 26 mS cm^{-1} and stable Zn electroplating/stripping as parallel platelets on the Zn anode at ultra-high current densities as high as 80 mA cm^{-2}. The side reactions caused by free water molecules, such as hydrogen evolution and the formation of a passivating $Zn_4SO_4(OH)_6 \cdot xH_2O$ layer, are also greatly reduced. We demonstrate a Zn||MnO_2 full battery based on this cellulose-CMC electrolyte showing excellent cyclability of over 500 cycles at a rate of 8 C. Additionally, the electrolyte requires minimal processing and is composed of inherently biodegradable materials without any synthetic additives from fossil fuels, suggesting its potential as a low-cost, sustainable, and high-performance electrolyte for next-generation energy storage applications.

2. Results and Discussion

2.1. Material Preparation and Characterization

The cellulose-CMC electrolyte is prepared using a simple process including vacuum filtration and NaOH treatment (Figure S1, Supporting Information). To fabricate the membrane, we first dispersed a commercial cellulose nanofiber gel

© 2023 The Authors. Advanced Functional Materials published by Wiley-VCH GmbH

16163028, 2023, 27, Downloaded from https://advanced.onlinelibrary.wiley.com/doi/10.1002/adfm.202302098, Wiley Online Library on [03/12/2025]. See the Terms and Conditions (https://onlinelibrary.wiley.com/terms-and-conditions) on Wiley Online Library for rules of use; OA articles are governed by the applicable Creative Commons License

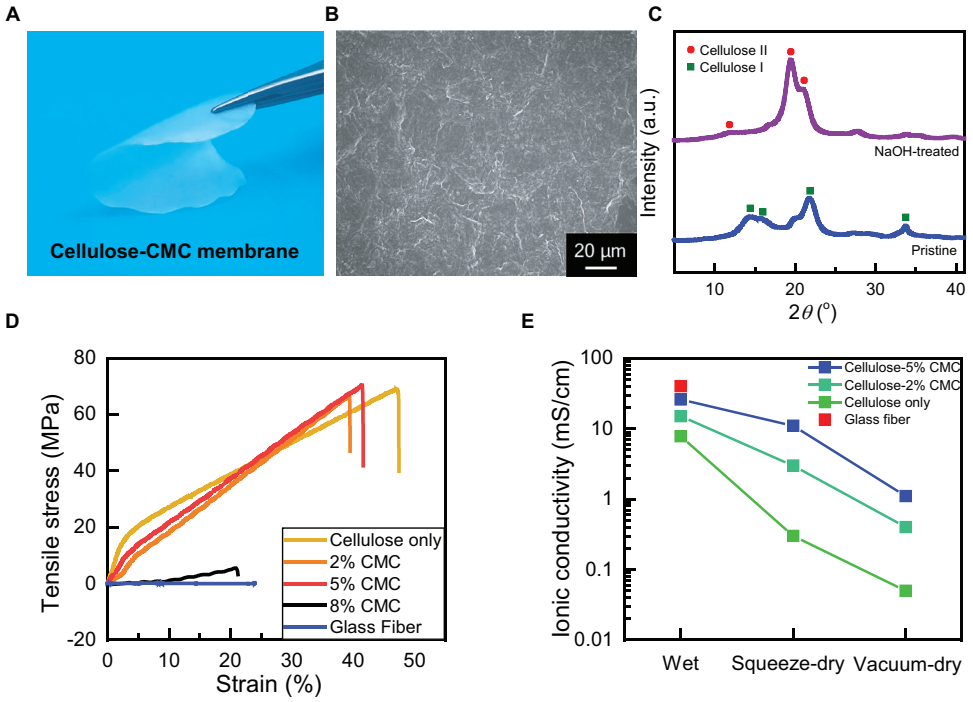

Figure 2. Characterization of the cellulose-5 wt.% CMC electrolyte. A) Digital image of the cellulose-CMC electrolyte. B) SEM image of the surface morphology of the cellulose-5 wt.% CMC electrolyte. C) XRD patterns of the cellulose-5 wt.% CMC membrane before and after NaOH treatment. D) Tensile tests of different NaOH-treated cellulose-CMC membranes (0–8 wt.%), as well as a glass fiber separator as a control. All membranes are in wet state. E) Ionic conductivity of a wet glass fiber separator, as well as various cellulose-CMC membranes (0–5 wt.% CMC) after different drying conditions: wet, squeezed dry by Kimwipes with 0.5 MPa pressure, and vacuum dried for 30 s. The thicknesses of the electrolytes were 80 μm.

(Figures S2A and S3, Supporting Information) within deionized (DI) water at a concentration of 0.1 wt.%, then slowly pipetted different masses of 0.5 wt.% CMC solution (Figure S2B, Supporting Information) into the dispersion to produce samples with different CMC contents (2, 5, and 8 wt.%). After thorough mixing, the resulting dispersions were vacuum-filtered through a Büchner funnel, collecting the pristine cellulose-CMC mixture on a filter membrane. Next, we immersed the membranes in NaOH solution (20 wt.%) overnight to improve their tensile strength.[42] We then rinsed the treated membranes with water until the pH of the washing solution reached 7. Finally, the membranes were immersed in a solution of 2 M $ZnSO_4$ to infiltrate the material with Zn^{2+} ions and were then squeezed between Kimwipes at a pressure of 0.5 MPa before cell assembly. The resulting cellulose-CMC electrolyte membranes were highly flexible (**Figure 2**A) and featured good hydrophilicity (Figure S4, Supporting Information). As a control, a pure cellulose membrane was prepared using the same procedure but without the addition of CMC solution (0 wt.% CMC).

We used scanning electron microscopy (SEM) and found the cellulose-CMC membranes featured a dense structure. For example, prior to NaOH treatment, the cellulose-5 wt.% CMC membrane featured no visible pores at the micrometer scale (Figure S5, Supporting Information) and remained intact after the NaOH treatment (Figure 2B; Figure S6, Supporting Information). We also note the electrochemical window of the cellulose-5 wt.% CMC electrolyte did not show significant change after the treatment (Figure S7, Supporting Information), indicating all remaining NaOH had been thoroughly rinsed away. However, the NaOH treatment did significantly improve the wet-state mechanical strength of the cellulose-based membrane, which is crucial for resisting perforation by Zn dendrites. As shown in Figure S8 (Supporting Information), the NaOH-treated cellulose-5 wt.% CMC membranes displayed tensile strengths of 72 ± 5 MPa in their wet state, which is much higher than that of the cellulose-5 wt.% CMC membrane before NaOH treatment (16 ± 4 MPa) and the commonly used glass fiber separator (0.12 ± 0.02 MPa), reaching higher or similar values as other hydrogel electrolytes.[24,43–45] The increase in strength is a result of the transformation of cellulose's molecular structure under NaOH treatment,[42] as we confirmed by X-ray diffraction (XRD). Prior to treatment, the pristine cellulose (Figure S9, Supporting Information) and cellulose-5 wt.% CMC membrane (Figure 2C) exhibit the XRD pattern of the cellulose I structure, which changes to match that of cellulose II after the NaOH treatment.[46] Previous studies have shown that membranes with cellulose II structure have higher tensile strength compared to those with cellulose I[42,47,48] as more intermolecular hydrogen bonds can be formed.[49] Therefore, the NaOH treatment helps improve the mechanical strength of the cellulose membrane, allowing it to serve as a strong background matrix for the CMC molecules without changing the functional groups of the biopolymers, as indicated by Fourier transform infrared (FTIR) spectroscopy (Figure S10, Supporting Information).

To determine an optimal amount of CMC added to the cellulose, we compared the tensile strength of the cellulose membranes featuring 0–8 wt.% CMC in their wet state (Figure 2D).

© 2023 The Authors. Advanced Functional Materials published by Wiley-VCH GmbH

16163028, 2023, 27, Downloaded from https://advanced.onlinelibrary.wiley.com/doi/10.1002/adfm.202302098, Wiley Online Library on [03/12/2025]. See the Terms and Conditions (https://onlinelibrary.wiley.com/terms-and-conditions) on Wiley Online Library for rules of use; OA articles are governed by the applicable Creative Commons License

The tensile strengths of the membranes fabricated with 0, 2, and 5 wt.% CMC were 72 ± 5, 67 ± 3, and 70 ± 5 MPa, respectively, while the tensile strength of the 8 wt.% CMC membrane decreased significantly to 5.4 ± 0.6 MPa. This decrease in strength is likely due to the increasingly-sparse distribution of the cellulose molecular chains. As a result, a cellulose-CMC membrane with a CMC content of 8 wt.% or higher would be very unlikely to prevent short circuits by dendritic growth, making it unsuitable as an electrolyte for ZIBs.

We then compared the Zn^{2+} conductivities of the 0–5 wt.% cellulose-CMC samples under different wet states using electrochemical impedance spectroscopy (EIS, Figure S11, Supporting Information) and plotted the calculated ionic conductivities in Figure 2E. When all three membranes were in a wet state, the ionic conductivity was 7.8, 15, and 26 mS cm^{-1} for the 0, 2, and 5 wt.% CMC samples, respectively. This trend indicates the enhancement of the conductivity by the addition of CMC. Moreover, after the three membranes were squeezed between Kimwipe tissues with an applied pressure of 0.5 MPa to remove some free water (squeeze-dry), the 5 wt.% CMC membrane retained a relatively high ionic conductivity of 11 mS cm^{-1}, while the 0 and 2 wt.% CMC membranes dropped to 0.3 and 3 mS cm^{-1}, respectively. Finally, in the extreme case, the squeeze-dried membranes were placed in a vacuum chamber for 30 s (vacuum-dry) to remove more water. After vacuum treatment, the cellulose-only membrane (0 wt.% CMC) had a negligible conductivity of 0.05 mS cm^{-1}, the 2 wt.% CMC sample featured a conductivity of 0.4 mS cm^{-1}, while the 5 wt.% CMC membrane retained a conductivity of 1.1 mS cm^{-1}.

We attribute the difference in the observed ionic conductivities to the varying ability of the membranes to retain water depending on their CMC content. Table S1 (Supporting Information) summarizes the water content of the samples, which we measured by monitoring the change in mass after the different drying conditions. In all three cases, the cellulose-5 wt.% CMC membrane retained more water than the other two samples, which is likely why it displayed better Zn^{2+} conductivity overall. The improved ability to retain water by adding CMC was also confirmed by both water retention (Figure S12, Supporting Information) and water uptake measurements (Table S2, Supporting Information). When no CMC was present, the membrane lost 50 wt.% of its water content within 10 min, while this time increased to ≈50 min for the 5 wt.% CMC sample. As a result, 5 wt.% was chosen as the optimal CMC percentage for further tests, attaining a balance between high mechanical strength and high ionic conductivity/ability to bond water molecules. However, further optimization may be possible for even better performance.

To better understand the Zn ion transport, we measured the transference numbers of both a glass fiber separator with 2 M $ZnSO_4$ solution and the cellulose-5 wt.% CMC electrolyte after squeezing it dry (Figure S13 and Table S3, Supporting Information). The transference number of the cellulose-5 wt.% CMC (0.39) was only slightly higher than that of the glass fiber separator using aqueous electrolyte (0.33), implying that the dissociation of Zn^{2+} in the cellulose-CMC electrolyte occurs in a similar way as in aqueous solution. Based on this result, we hypothesize that Zn^{2+} ions experience a similar environment in the cellulose-CMC sample as in bulk water, suggesting the Zn ions are fully solvated in the membrane. We hypothesize ion conduction may take place along channels formed by water molecules coordinated to the CMC molecules. However, additional studies are necessary to confirm this structure.

2.2. Electrodeposition and Stripping of Zn

Using Zn‖Zn symmetric cells fabricated with cellulose-5 wt.% CMC electrolyte, we tested the electrodeposition and stripping performance of Zn and compared it to a cell fabricated using a glass fiber separator and aqueous electrolyte (2 M $ZnSO_4$ in deionized water). Both samples were cycled at a current density of 10 mA cm^{-2} and a capacity density of 5 mAh cm^{-2} for 50 cycles. After cycling, the Zn foils were removed from the cell for post-mortem SEM analysis. When Zn was plated using the aqueous electrolyte and glass fiber separator, we found Zn platelets grew perpendicular to the surface of the Zn foil (**Figure 3**A). In contrast, using the cellulose-5 wt.% CMC electrolyte, we observed the formation of hexagonal Zn platelets oriented parallel to the Zn electrode surface (Figure 3B). These results suggest the ability of the cellulose-5 wt.% CMC electrolyte to reduce Zn dendrite formation. We also performed XRD measurements on both samples, as well as pristine Zn foil for comparison. As shown in Figure 3C, after cycling using the cellulose-5 wt.% CMC electrolyte, we observe an increase in the relative intensity of the XRD peak corresponding to the (002) planes (2θ = 36°) of Zn (Table S4, Supporting Information), which previous studies have shown is preferred for Zn growth parallel to the electrode surface.[50,51] These results further demonstrate the preferred parallel growth of Zn platelets during electrodeposition.

The electrodeposition and stripping of Zn in the battery are likely impacted by multiple effects. For example, when using the aqueous electrolyte and glass separator, the Zn growth does not face much mechanical resistance, thus enabling the perpendicular orientation of the Zn platelets (Figure 3D), which could promote dendritic growth. In contrast, the high mechanical strength and dense structure of the cellulose-5 wt.% CMC membrane inhibits the perpendicular growth of Zn, mechanically constraining the deposition within the narrow gap between the membrane surface and Zn foil such that parallel growth is preferred (Figure 3E). Additionally, Zn^{2+} can migrate freely within the aqueous electrolyte (Figure 3D). As a result, Zn ions will accumulate at regions of the electrode where the surface is rougher, creating "hot-spots" of deposition due to the higher concentrated electric field. This positive feedback will accelerate the perpendicular growth of Zn, which is the cause of dendrite formation in many other electrodeposition systems, such as Li-metal batteries.[52] In contrast, the CMC chains within the cellulose-5 wt.% CMC electrolyte may help bond water molecules within the electrolyte, which could promote the migration of Zn ions along the CMC chains. Consequently, the Zn ions may distribute more evenly on the surface of the Zn foil rather than accumulate around potential "hot-spots." Finally, as illustrated by the XRD pattern (Figure 3C), $Zn_4SO_4(OH)_6 \cdot xH_2O$ forms after cycling in aqueous electrolyte (peaks labeled by green squares). Due to the large free water content in the aqueous electrolyte, a $Zn_4SO_4(OH)_6 \cdot xH_2O$ passivation layer

© 2023 The Authors. Advanced Functional Materials published by Wiley-VCH GmbH

16163028, 2023, 27, Downloaded from https://advanced.onlinelibrary.wiley.com/doi/10.1002/adfm.202302098, Wiley Online Library on [03/12/2025]. See the Terms and Conditions (https://onlinelibrary.wiley.com/terms-and-conditions) on Wiley Online Library for rules of use; OA articles are governed by the applicable Creative Commons License

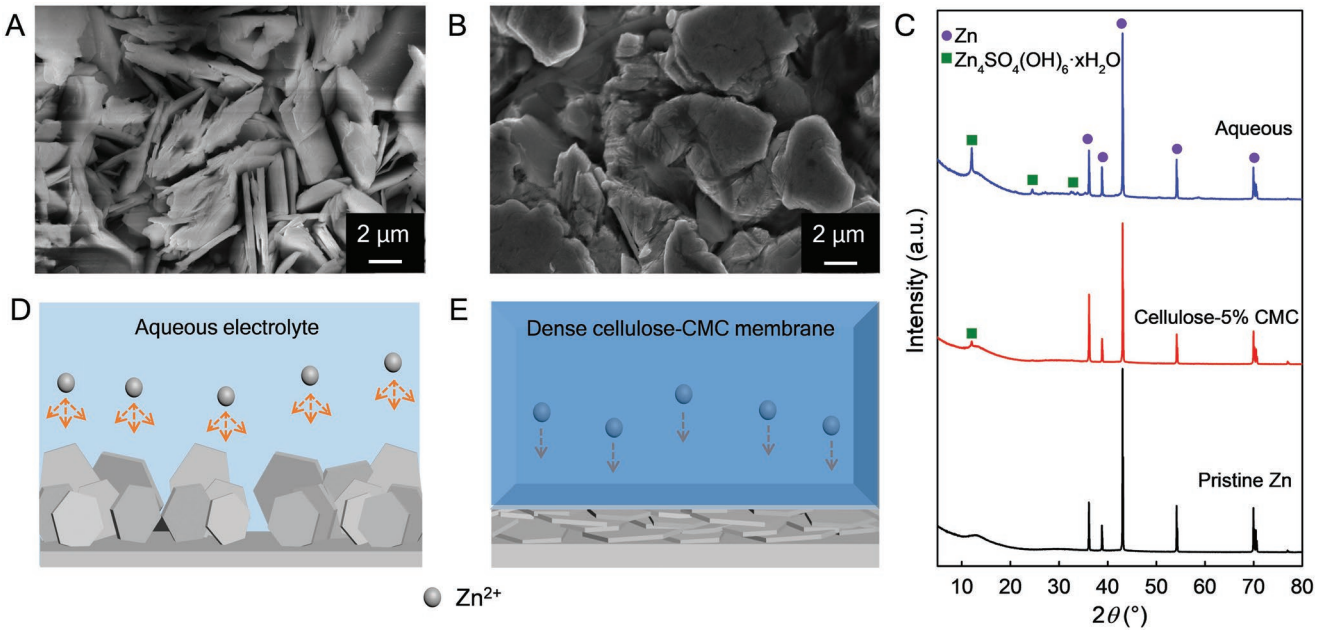

Figure 3. Reduction of the dendritic growth of Zn by the cellulose-5 wt.% CMC membrane. A,B) The morphology of Zn plating on the Zn anode after cycling at 10 mA cm^{-2} and 5 mAh cm^{-2} for 50 cycles in Zn||Zn cells fabricated with A) 2 M $ZnSO_4$ aqueous electrolyte with a glass fiber separator and B) cellulose-5 wt.% CMC electrolyte. C) XRD patterns of the Zn foils after cycling with the 2 M $ZnSO_4$ aqueous electrolyte (with glass fiber separator) and the cellulose-5 wt.% CMC electrolyte, as well as a pristine Zn foil without cycling. Schematic diagrams of Zn plating on the Zn anode using the D) aqueous electrolyte and E) cellulose-5 wt.% CMC electrolyte.

forms on the surface of the Zn foil. The $Zn_4SO_4(OH)_6 \cdot xH_2O$ byproduct is electrochemically inert and will prevent further Zn deposition.[53] However, thanks to the strong bonding between CMC and water molecules[40] within the cellulose-5 wt.% CMC electrolyte, there is reduced formation of $Zn_4SO_4(OH)_6 \cdot xH_2O$ (Figure 3C), allowing Zn to deposit over the entire Zn foil surface throughout cycling. All combined, these advantages of the cellulose-5 wt.% CMC electrolyte help suppress the dendritic, perpendicular growth of Zn, enabling stable and reversible Zn plating/stripping.

As shown in **Figure 4**, excellent Zn||Zn cycling performance is achieved using the cellulose-5 wt.% CMC electrolyte. With a current density of 10 mA cm^{-2} and capacity of 5 mAh cm^{-2}, a symmetric cell with cellulose-5 wt.% CMC electrolyte showed a polarization voltage of 50 mV (Figure 4A, red), remaining approximately constant throughout 350 cycles. In contrast, using aqueous electrolyte with the glass fiber separator, the initial polarization is as large as 100 mV and quickly approaches an irreversible and dramatic increase after 30 cycles (Figure 4A, grey). This comparison indicates that the Zn anode interface using the cellulose-5 wt.% CMC electrolyte has much greater durability. In addition to the stark difference in the polarization voltage behavior, the cell made with the aqueous electrolyte visibly swells after 160 cycles at 10 mA cm^{-2} and 5 mAh cm^{-2} (Figure S14A, Supporting Information). The inflation of the coin cell is likely caused by the hydrogen evolution reaction with free water molecules, which occurs on the Zn anode.[54] Conversely, the cell with the cellulose-5 wt.% CMC electrolyte has no observable volumetric swelling after 350 cycles (Figure S14B, Supporting Information). The cellulose-CMC electrolyte bonds to water molecules strongly, and thus it appears to mitigate the long-standing issue of hydrogen evolution in aqueous Zn batteries.

With the cellulose-5 wt.% CMC electrolyte, we successfully cycled Zn symmetric cells at 80 mA cm^{-2} (4 mAh cm^{-2}, 3500 cycles, Figure 4B) and 40 mA cm^{-2} (8 mAh cm^{-2}, 2200 cycles, Figure S15, Supporting Information), with a cumulative plating capacity of 14 and 17.6 Ah cm^{-2}, respectively. These results outperform previously reported Zn symmetric cells in terms of current density as well as cumulative plating capacity, including cells using hydrogel electrolytes and Zn salt with different additives (Figure 4C), demonstrating the excellent potential of the cellulose-5 wt.% CMC electrolyte for ultra-fast charging-discharging of Zn-metal anodes. Additionally, we note the tensile strength did not change significantly after cycling (Figure S16, Supporting Information), demonstrating the mechanical durability of the electrolyte. However, during cycling we observed the polarization first decreased and then increased (Figure 4B). To understand this behavior, we performed EIS measurements at the beginning and after 1700 and 3400 cycles, where we found that the interfacial resistance first decreased, then increased (Figure S17, Supporting Information). This evolution of the interfacial resistance could possibly be ascribed to the fact that during the initial cycles some interfacial activation occurred, which later improves the interfacial contact between the electrolyte and Zn foil. Then during further cycles, although significantly reduced, some surface passivation species (e.g., $Zn_4SO_4(OH)_6 \cdot xH_2O$) still form on the surface of the Zn foil, as can be seen in the XRD results shown in Figure 3C. This passivation layer may have resulted in the increasing polarization in the later stage of cycling. In addition, by comparing the x-intercept of the EIS spectra (Figure S17B, Supporting

© 2023 The Authors. Advanced Functional Materials published by Wiley-VCH GmbH

16163028, 2023, 27, Downloaded from https://advanced.onlinelibrary.wiley.com/doi/10.1002/adfm.202302098, Wiley Online Library on [03/12/2025]. See the Terms and Conditions (https://onlinelibrary.wiley.com/terms-and-conditions) on Wiley Online Library for rules of use; OA articles are governed by the applicable Creative Commons License

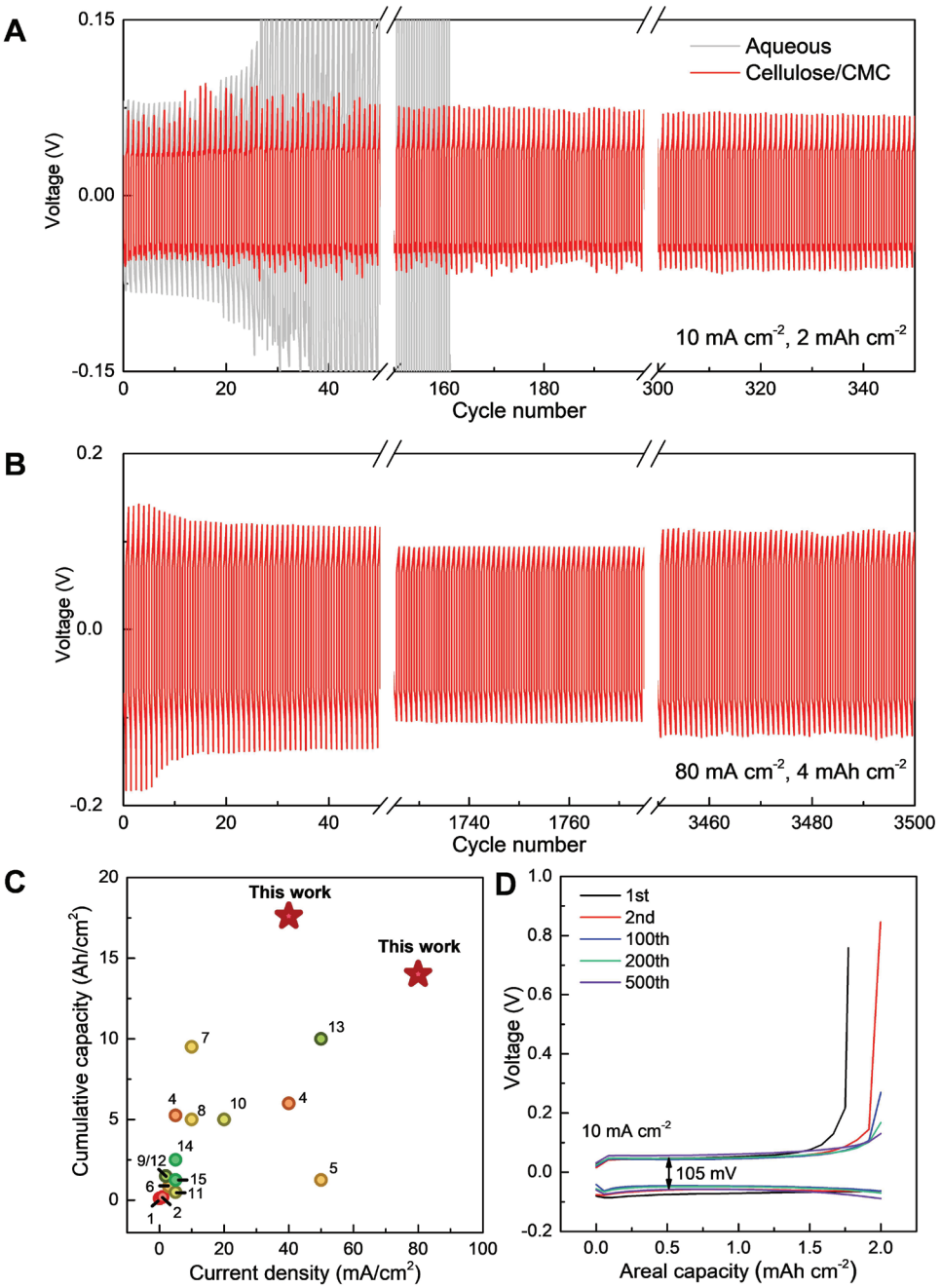

Figure 4. Electrochemical performance of Zn plating/stripping. A) The Zn plating/stripping of a Zn||Zn symmetric cell at 10 mA cm^{-2} and 5 mAh cm^{-2} using the cellulose-5 wt.% CMC electrolyte (red line) and aqueous electrolyte with glass fiber separator (grey line). B) The Zn plating/stripping of a Zn||Zn symmetric cell at 80 mA cm^{-2} and 4 mAh cm^{-2} using the cellulose-5 wt.% CMC electrolyte. C) Performance comparison of the Zn||Zn symmetric cell in terms of the current density and cumulative capacity cycled using the cellulose-5 wt.% CMC electrolyte and other reported electrolytes.[22,31,55–67] D) The Zn plating/stripping of a Zn||Cu asymmetric cell at 10 mA cm^{-2} and 2 mAh cm^{-2}.

Information), it was found that the bulk resistivity increased ≈25% after cycling, indicating that the bulk ionic conductivity decreases 20%. This could be due to the consumption of bound water during cycling.

Using the cellulose-5 wt.% CMC electrolyte, we also tested the electrodeposition of Zn on Cu foil using a Zn||Cu asymmetric cell at 10 mA cm^{-2} with a capacity of 2 mAh cm^{-2} and a cutoff voltage of 0.8 V (Figure 4D). The cell showed a high average Coulombic efficiency of 99.5% over 500 cycles (Figure S18, Supporting Information) with a smaller voltage hysteresis of 105 mV. Both the Zn||Zn and Zn||Cu cells demonstrate the high stability, cyclability, and capability of the cellulose-5 wt.% CMC electrolyte to withstand a high current density, all of which is crucial for high power density aqueous ZIBs.

© 2023 The Authors. Advanced Functional Materials published by Wiley-VCH GmbH

16163028, 2023, 27, Downloaded from https://advanced.onlinelibrary.wiley.com/doi/10.1002/adfm.202302098, Wiley Online Library on [03/12/2025]. See the Terms and Conditions (https://onlinelibrary.wiley.com/terms-and-conditions) on Wiley Online Library for rules of use; OA articles are governed by the applicable Creative Commons License

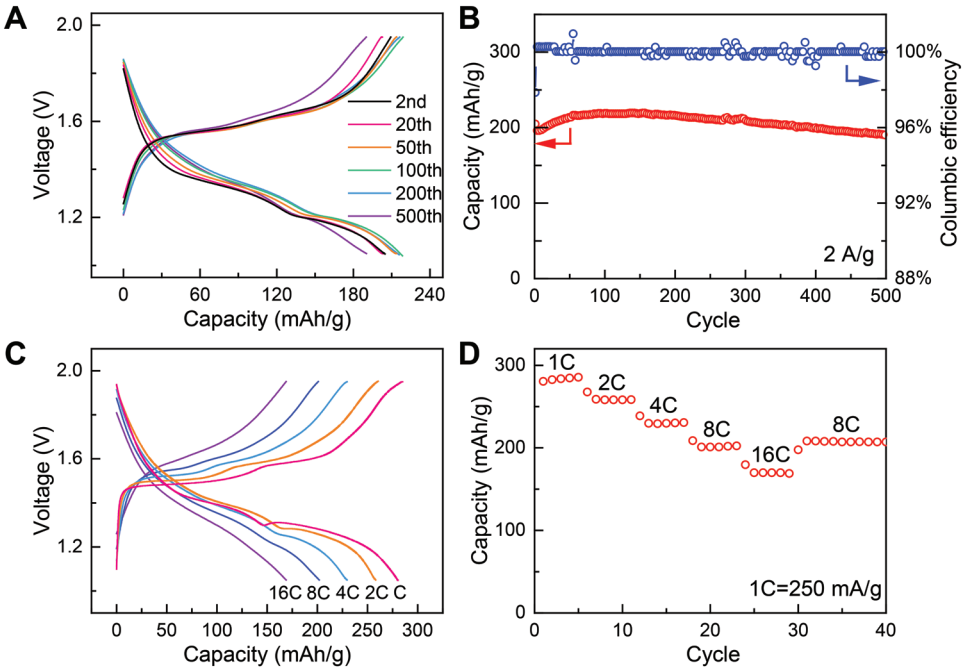

Figure 5. Electrochemical performance of Zn||MnO_2 full cells using the cellulose-5 wt.% CMC electrolyte. A) Galvanostatic charge-discharge potential profiles of the Zn||MnO_2 cell using cellulose-5 wt.% CMC electrolyte at 8 C. B) Capacity and coulombic efficiency of the Zn||MnO_2 cell using cellulose-5 wt.% CMC electrolyte at 8 C. C) Galvanostatic charge-discharge potential profiles of the Zn||MnO_2 cell using cellulose-5 wt.% CMC electrolyte at various rates. D) Rate performance of the Zn||MnO_2 cell using cellulose-5 wt.% CMC electrolyte ranging from 1 C to 16 C.

2.3. Zn||MnO_2 Full Cell Performance

We used the conventional Zn||MnO_2 chemistry[68] to evaluate the performance of the cellulose-5 wt.% CMC electrolyte in full cells. MnO_2 nanorods were synthesized using a hydrothermal method[69] (Figure S19, Supporting Information) and cast onto carbon paper as the cathode. The mass loading of MnO_2 was ≈6 mg cm^{-2}. As shown in **Figure 5**A, the Zn||MnO_2 full cell exhibits a high discharge/charge capacity of ≈200 mAh g^{-1} at an ultra-high rate of 8C (1C = 250 mA g^{-1}). Additionally, a high-capacity retention of 95% was achieved after 500 cycles (Figure 5B). The battery experienced no short-circuit during this high-rate cycling, suggesting the inhibition of dendritic growth by the cellulose-5 wt.% CMC electrolyte.

The Zn||MnO_2 battery also demonstrates outstanding rate performance both in terms of discharge profile (Figure 5C) and cycling performance (Figure 5D), delivering discharge capacities of 284, 258, 230, and 201 mAh g^{-1} at 1 C, 2 C, 4 C, and 8 C, respectively. Even at a high rate of 16 C, a discharge capacity of 170 mAh g^{-1} was achieved. We also compared the cycling performance of the cellulose-5 wt.% CMC electrolyte to the cellulose-only electrolyte (0% CMC), as well as the aqueous electrolyte/glass fiber separator, where the cellulose-5 wt.% CMC electrolyte demonstrated the best performance (Figure S20, Supporting Information). Moreover, the capacity retention of the cellulose-5 wt.% CMC cell is high compared to other previously reported bio-based electrolytes for ZIBs (Table S5, Supporting Information). These results clearly demonstrate the strong performance and compatibility of the cellulose-CMC electrolyte with the most commonly studied and low-cost Zn||MnO_2 chemistry.

3. Conclusion

In this work, we demonstrate the excellent performance of a cellulose-CMC electrolyte for aqueous ZIBs. The cellulose-CMC electrolyte is derived from easily-accessible, low-cost natural materials, with no synthetic additives from fossil fuels, and was fabricated via a facile mixing and vacuum filtration method, followed by a simple NaOH treatment. The cellulose-CMC electrolyte with 5 wt.% CMC exhibits a high mechanical strength of up to 70 MPa and excellent ability to bond water molecules,[42] resulting in not only high ionic conductivity but also fewer side reactions. These properties enable the ultra-fast electroplating/stripping of Zn, largely free of the formation of dendrites and side reactions, at a current density up to 80 mA cm^{-2} for more than 3500 cycles. Zn||MnO_2 full cells fabricated with the cellulose-CMC electrolyte show excellent cyclability (95% capacity retention after 500 cycles at 8C) and rate performance with a rate of up to 16 C. Considering the low cost, sustainability, inherent safety (compared to flammable organic-based systems, with low risk of thermal runaway, Figure S21, Supporting Information), facile fabrication, and the extraordinary electrochemical performance and compatibility with simple Zn||MnO_2 chemistry, the cellulose-CMC electrolyte has great potential for Zn ion batteries, paving the way toward grid-scale energy storage for renewable energy sources.

© 2023 The Authors. Advanced Functional Materials published by Wiley-VCH GmbH

16163028, 2023, 27, Downloaded from https://advanced.onlinelibrary.wiley.com/doi/10.1002/adfm.202302098, Wiley Online Library on [03/12/2025]. See the Terms and Conditions (https://onlinelibrary.wiley.com/terms-and-conditions) on Wiley Online Library for rules of use; OA articles are governed by the applicable Creative Commons License

4. Experimental Section

Materials: Cellulose nanofiber gel (3 wt.%) was purchased from SAPPI. Carboxymethyl cellulose (CMC) powder (400000 g mol^{-1}), polyvinylidene fluoride (PVDF) powder (>99.5%), and zinc foil (100 µm in thickness, 99.9%) were purchased from MTI corporation. Sodium hydroxide (NaOH, 97%), Zinc sulfate heptahydrate (99%), N-methyl-2-pyrrolidone (NMP, 99.5%), ammonium persulfate (98%), and Manganese(II) sulfate monohydrate (>98%) were purchased from Millipore Sigma. All materials were used directly without any treatment.

Preparation of the Cellulose-CMC Membrane: CMC was first dissolved in DI water by stirring overnight at room temperature to produce a 0.5 wt.% CMC solution. Then 1.33 g of 3 wt.% cellulose nanofiber gel was added to 40 mL DI water. After that, 0, 16, 42, or 69 mg of 0.5 wt.% CMC solution was slowly pipetted into the dispersion to produce samples with 0 wt.%, 2 wt.%, 5 wt.%, and 8 wt.% CMC contents. The dispersion was mixed using a vortex mixer for 10 min, then bath sonicated for 30 min, which yielded a uniform dispersion with no visible aggregation. The dispersion was then vacuum filtrated through a PVDF filter membrane (Durapore, 0.65 µm pore size), which yielded a wet cellulose-CMC film that could be easily peeled off from the filter. The film was immediately immersed in 20 wt.% NaOH solution for 12 h, then rinsed with DI water until the rinsing solution reached pH 7. The membrane was stored in DI water for further treatment.

Preparation of the Cellulose-CMC Electrolyte: The cellulose-CMC membrane was immersed in 2 M $ZnSO_4$ aqueous solution overnight for Zn plating/stripping tests, or immersed in 2 M $ZnSO_4$/0.1 M $MnSO_4$ aqueous solution overnight for Zn||MnO_2 full cell tests. The cellulose-CMC electrolyte was obtained after squeezing between Kimwipes with a pressure of 0.5 MPa (squeeze-dry).

Water Uptake and Water Retention Measurements: To measure the water uptake, the membranes were first dried in a vacuum oven at 100 °C for 12 h to remove all water, and then soaked in deionized water for 1 h. The water uptake was defined by the ratio between the mass of the dry membrane and the mass of the soaked membranes. For water retention tests, the soaked membranes were placed in an ambient environment of 25 °C and 1% relative humidity. Then the masses of the membranes were measured every 20 min and recorded.

EIS Tests: EIS tests were performed with stainless steel plates as blocking electrodes. The cellulose-CMC electrolyte was sandwiched between two stainless steel plates and then assembled within a CR2032 coin cell for EIS measurements. The cellulose-CMC electrolyte had a thickness of 80 µm. The EIS data was measured using a Biologic VMP3 electrochemical workstation at an amplitude of 10 mV at an open circuit voltage.

Transference Number Measurement: The Zn^{2+} transference numbers were measured using the Bruce–Vincent method. DC polarization measurements were conducted with a potential of ΔV = 10 mV in the Zn||Zn cells until the current reached a steady state, and corresponding EIS measurements were collected before and after the DC polarization. The Zn^{2+} transference number (t_{Zn}) was calculated according to:

$$t_{Zn} = \frac{I_{SS}\left(\Delta V - I_0 R_0\right)}{I_0\left(\Delta V - I_{SS} R_{SS}\right)} \quad (1)$$

where ΔV is the applied potential, I_0 is the initial current, R_0 is the initial resistance, I_{ss} is the steady-state current, and R_{ss} is the steady-state resistance.

Electrochemical Tests for Zn Plating/Stripping: Zn symmetric cells were assembled using Zn foils for both the cathode and anode, and either the cellulose-CMC electrolyte or aqueous electrolyte (100 µL 2 M $ZnSO_4$) with a glass fiber separator. The asymmetric Cu||Zn cells were assembled using Cu foil and Zn foil as the cathode and anode. All cells were assembled in ambient environment using CR2032 coin cells and tested at room temperature. The galvanostatic plating/stripping profiles were measured by a NEWARE battery testing system.

Electrochemical Tests for Zn||MnO_2 Full Cell: MnO_2 nanorods were synthesized by a hydrothermal method reported in the literature.[69] To prepare composite electrodes, MnO_2, Ketjenblack EC-600JD, and PVDF were mixed at a mass ratio of 8:1:1 within NMP. The resulting slurry was then cast onto carbon paper and dried at 100 °C under vacuum for 12 h before cell assembly. The areal loading of the active material was ≈6 mg cm^{-2}. The electrochemical performances of the composite electrodes were evaluated in a CR2032 coin cell with a zinc foil anode and cellulose-CMC electrolyte ($ZnSO_4$/$MnSO_4$). The galvanostatic charging/discharging profiles were measured by a NEWARE battery testing system. All electrochemical tests were run at room temperature.

Supporting Information

Supporting Information is available from the Wiley Online Library or from the author.

Acknowledgements

The authors acknowledge support from the US Department of Energy (DOE), Advanced Research Projects Agency – Energy (ARPA-E), under award no. DE-AR0001588. The authors acknowledge the support of the University of Maryland A. James Clark School of Engineering.

Conflict of Interest

The authors declare no conflict of interest.

Data Availability Statement

The data that support the findings of this study are available from the corresponding author upon reasonable request.

Keywords

biopolymeric electrolytes, carboxymethyl cellulose, high-rate performance, nano-cellulose, Zn ion batteries

Received: March 2, 2023
Published online: April 2, 2023

[1] F. Creutzig, P. Jochem, O. Y. Edelenbosch, L. Mattauch, D. P. van Vuuren, D. McCollum, J. Minx, *Science* **2015**, *350*, 911.
[2] J.-M. Tarascon, *Nat. Mater.* **2022**, *21*, 979.
[3] X. Yu, A. Manthiram, *Adv. Energy Sustainability Res.* **2021**, *2*, 2000102.
[4] C. Xia, J. Guo, Y. Lei, H. Liang, C. Zhao, H. N. Alshareef, *Adv. Mater.* **2018**, *30*, 1705580.
[5] Y. Zhang, Z. Chen, H. Qiu, W. Yang, Z. Zhao, J. Zhao, G. Cui, *NPG Asia Mater.* **2020**, *12*, 4.
[6] D. Chao, W. Zhou, F. Xie, C. Ye, H. Li, M. Jaroniec, S.-Z. Qiao, *Sci. Adv.* **2020**, *6*, eaba4098.
[7] P. Xu, D. H. S. Tan, Z. Chen, *Trends Chem.* **2021**, *3*, 620.
[8] T. Zhang, Y. Tang, S. Guo, X. Cao, A. Pan, G. Fang, J. Zhou, S. Liang, *Energy Environ. Sci.* **2020**, *13*, 4625.
[9] L. E. Blanc, D. Kundu, L. F. Nazar, *Joule* **2020**, *4*, 771.
[10] B. Yong, D. Ma, Y. Wang, H. Mi, C. He, P. Zhang, *Adv. Energy Mater.* **2020**, *10*, 2002354.
[11] V. Verma, S. Kumar, W. Manalastas, M. Srinivasan, *ACS Energy Lett.* **2021**, *6*, 1773.
[12] L. Kang, M. Cui, F. Jiang, Y. Gao, H. Luo, J. Liu, W. Liang, C. Zhi, *Adv. Energy Mater.* **2018**, *8*, 1801090.

© 2023 The Authors. Advanced Functional Materials published by Wiley-VCH GmbH

16163028, 2023, 27, Downloaded from https://advanced.onlinelibrary.wiley.com/doi/10.1002/adfm.202302098, Wiley Online Library on [03/12/2025]. See the Terms and Conditions (https://onlinelibrary.wiley.com/terms-and-conditions) on Wiley Online Library for rules of use; OA articles are governed by the applicable Creative Commons License

[13] D. J. Arnot, M. B. Lim, N. S. Bell, N. B. Schorr, R. C. Hill, A. Meyer, Y. T. Cheng, T. N. Lambert, *Adv. Energy Mater.* **2021**, *11*, 2101594.
[14] C. Ma, K. Yang, S. Zhao, Y. Xie, C. Liu, N. Chen, C. Wang, D. Wang, D. Zhang, Z. X. Shen, F. Du, *ACS Energy Lett.* **2023**, *8*, 1201.
[15] C. Chen, K. Matsumoto, K. Kubota, R. Hagiwara, Q. Xu, *Adv. Energy Mater.* **2019**, *9*, 1900196.
[16] F. Wang, O. Borodin, T. Gao, X. Fan, W. Sun, F. Han, A. Faraone, J. A. Dura, K. Xu, C. Wang, *Nat. Mater.* **2018**, *17*, 543.
[17] H. Yang, Z. Chang, Y. Qiao, H. Deng, X. Mu, P. He, H. Zhou, *Angew. Chem., Int. Ed.* **2020**, *59*, 9377.
[18] A. Naveed, H. Yang, J. Yang, Y. Nuli, J. Wang, *Angew. Chem., Int. Ed.* **2019**, *58*, 2760.
[19] N. Wang, Y. Yang, X. Qiu, X. Dong, Y. Wang, Y. Xia, *ChemSusChem* **2020**, *13*, 5556.
[20] Y. Ding, Z. Pang, K. Lan, Y. Yao, G. Panzarasa, L. Xu, M. Lo Ricco, D. R. Rammer, J. Y. Zhu, M. Hu, X. Pan, T. Li, I. Burgert, L. Hu, *Chem. Rev.* **2022**, *123*, 1843.
[21] Q. Dong, X. Zhang, J. Qian, S. He, Y. Mao, A. H. Brozena, Y. Zhang, T. P. Pollard, O. A. Borodin, Y. Wang, B. S. Chava, S. Das, P. Zavalij, C. U. Segre, D. Zhu, L. Xu, Y. Liang, Y. Yao, R. M. Briber, T. Li, L. Hu, *Sci. Adv.* **2022**, *8*, eadd2031.
[22] Z. Yang, W. Li, Q. Zhang, C. Xie, H. Ji, Y. Tang, Y. Li, H. Wang, *Mater. Today Energy* **2022**, *28*, 101076.
[23] J. Zhou, R. Zhang, R. Xu, Y. Li, W. Tian, M. Gao, M. Wang, D. Li, X. Liang, L. Xie, K. Liang, P. Chen, B. Kong, *Adv. Funct. Mater.* **2022**, *32*, 2111406.
[24] L. Ma, S. Chen, D. Wang, Q. Yang, F. Mo, G. Liang, N. Li, H. Zhang, J. A. Zapien, C. Zhi, *Adv. Energy Mater.* **2019**, *9*, 1803046.
[25] W. Xu, C. Liu, Q. Wu, W. Xie, W. Y. Kim, S. Y. Lee, J. Gwon, *J. Mater. Chem. A* **2020**, *8*, 18327.
[26] J. Fu, H. Wang, P. Xiao, C. Zeng, Q. Sun, H. Li, *Energy Storage Mater.* **2022**, *48*, 191.
[27] H. Glatz, E. Lizundia, F. Pacifico, D. Kundu, *ACS Appl. Energy Mater.* **2019**, *2*, 1288.
[28] M. Xu, H. Dou, Z. Zhang, Y. Zheng, B. Ren, Q. Ma, G. Wen, D. Luo, A. Yu, L. Zhang, X. Wang, Z. Chen, *Angew. Chem., Int. Ed.* **2022**, *61*, 202117703.
[29] Y. Zhang, Y. Chen, X. Li, M. Alfred, D. Li, F. Huang, Q. Wei, *J. Power Sources* **2021**, *482*, 228963.
[30] N. Zhao, F. Wu, Y. Xing, W. Qu, N. Chen, Y. Shang, M. Yan, Y. Li, L. Li, R. Chen, *ACS Appl. Mater. Interfaces* **2019**, *11*, 15537.
[31] J. Cao, D. Zhang, C. Gu, X. Zhang, M. Okhawilai, S. Wang, J. Han, J. Qin, Y. Huang, *Nano Energy* **2021**, *89*, 106322.
[32] W. Zhou, M. Chen, Q. Tian, J. Chen, X. Xu, C. P. Wong, *Energy Storage Mater.* **2022**, *44*, 57.
[33] Y. Guo, W. Cai, Y. Lin, Y. Zhang, S. Luo, K. Huang, H. Wu, Y. Zhang, *Energy Storage Mater.* **2022**, *50*, 580.
[34] P. Yang, J. Li, S. W. Lee, H. J. Fan, *Adv. Sci.* **2022**, *9*, 2103894.
[35] X. Ge, W. Zhang, F. Song, B. Xie, J. Li, J. Wang, X. Wang, J. Zhao, G. Cui, *Adv. Funct. Mater.* **2022**, *32*, 2200429.
[36] J. Cao, D. Zhang, C. Gu, X. Wang, S. Wang, X. Zhang, J. Qin, Z. Wu, *Adv. Energy Mater.* **2021**, *11*, 2101299.
[37] X. Zhang, J. Li, D. Liu, M. Liu, T. Zhou, K. Qi, L. Shi, Y. Zhu, Y. Qian, *Energy Environ. Sci.* **2021**, *14*, 3120.
[38] D. Wang, H. Li, Z. Liu, Z. Tang, G. Liang, F. Mo, Q. Yang, L. Ma, C. Zhi, *Small* **2018**, *14*, 1803978.
[39] L. Yang, L. Song, Y. Feng, M. Cao, P. Zhang, X. F. Zhang, J. Yao, *J. Mater. Chem. A* **2020**, *8*, 12314.
[40] K. Boruvkova, J. Wiener, *Autex Res. J.* **2011**, *11*, 110.
[41] W. J. Zheng, J. Gao, Z. Wei, J. Zhou, Y. M. Chen, *Eur. Polym. J.* **2015**, *72*, 514.
[42] K. Abe, H. Yano, *Cellulose* **2012**, *19*, 1907.
[43] Y. S. Zhu, S. Y. Xiao, M. X. Li, Z. Chang, F. X. Wang, J. Gao, Y. P. Wu, *J. Power Sources* **2015**, *288*, 368.
[44] M. Chen, J. Chen, W. Zhou, J. Xu, C.-P. Wong, *J. Mater. Chem. A* **2019**, *7*, 26524.
[45] H. Li, Z. Liu, G. Liang, Y. Huang, Y. Huang, M. Zhu, Z. Pei, Q. Xue, Z. Tang, Y. Wang, B. Li, C. Zhi, *ACS Nano* **2018**, *12*, 3140.
[46] J. Gong, J. Li, J. Xu, Z. Xiang, L. Mo, *RSC Adv.* **2017**, *7*, 33486.
[47] F. Fahma, F. A. Lestari, I. A. Kartika, N. Lisdayana, E. S. Iriani, *Karbala Int. J. Mod. Sci.* **2021**, *7*, 3.
[48] A. Tarbuk, A. M. Grancaric, M. Leskovac, *Cellulose* **2014**, *21*, 2167.
[49] M. Ferro, A. Mannu, W. Panzeri, C. H. J. Theeuwen, A. Mele, *Polymers* **2020**, *12*, 1559.
[50] M. Zhou, S. Guo, J. Li, X. Luo, Z. Liu, T. Zhang, X. Cao, M. Long, B. Lu, A. Pan, G. Fang, J. Zhou, S. Liang, *Adv. Mater.* **2021**, *33*, 2100187.
[51] Y. Liu, J. Hu, Q. Lu, M. Hantusch, H. Zhang, Z. Qu, H. Tang, H. Dong, O. G. Schmidt, R. Holze, M. Zhu, *Energy Storage Mater.* **2022**, *47*, 98.
[52] B. Zhang, L. Qin, Y. Fang, Y. Chai, X. Xie, B. Lu, S. Liang, J. Zhou, *Sci. Bull.* **2022**, *67*, 955.
[53] Q. Yang, L. Li, T. Hussain, D. Wang, L. Hui, Y. Guo, G. Liang, X. Li, Z. Chen, Z. Huang, Y. Li, Y. Xue, Z. Zuo, J. Qiu, Y. Li, C. Zhi, *Angew. Chem., Int. Ed.* **2022**, *61*, 202112304.
[54] L. Wang, W. Huang, W. Guo, Z. H. Guo, C. Chang, L. Gao, X. Pu, *Adv. Funct. Mater.* **2022**, *32*, 2108533.
[55] J. Zhao, J. Zhang, W. Yang, B. Chen, Z. Zhao, H. Qiu, S. Dong, X. Zhou, G. Cui, L. Chen, *Nano Energy* **2019**, *57*, 625.
[56] M. Zhu, X. Wang, H. Tang, J. Wang, Q. Hao, L. Liu, Y. Li, K. Zhang, O. G. Schmidt, *Adv. Funct. Mater.* **2020**, *30*, 1907218.
[57] P. Liang, J. Yi, X. Liu, K. Wu, Z. Wang, J. Cui, Y. Liu, Y. Wang, Y. Xia, J. Zhang, *Adv. Funct. Mater.* **2020**, *30*, 1908528.
[58] Y. Yin, S. Wang, Q. Zhang, Y. Song, N. Chang, Y. Pan, H. Zhang, X. Li, *Adv. Mater.* **2020**, *32*, 1906803.
[59] W. Guo, Y. Zhang, X. Tong, X. Wang, L. Zhang, X. Xia, J. Tu, *Mater. Today Energy* **2021**, *20*, 100675.
[60] L. Qian, W. Yao, R. Yao, Y. Sui, H. Zhu, F. Wang, J. Zhao, C. Zhi, C. Yang, *Adv. Funct. Mater.* **2021**, *31*, 2105736.
[61] P. Cao, X. Zhou, A. Wei, Q. Meng, H. Ye, W. Liu, J. Tang, J. Yang, *Adv. Funct. Mater.* **2021**, *31*, 2100398.
[62] H. Yan, S. Li, Y. Nan, S. Yang, B. Li, *Adv. Energy Mater.* **2021**, *11*, 2100186.
[63] L. Ma, S. Chen, N. Li, Z. Liu, Z. Tang, J. A. Zapien, S. Chen, J. Fan, C. Zhi, *Adv. Mater.* **2020**, *32*, 1908121.
[64] S. S. Shinde, J. Y. Jung, N. K. Wagh, C. H. Lee, D. H. Kim, S. H. Kim, S. U. Lee, J. H. Lee, *Nat. Energy* **2021**, *6*, 592.
[65] G. Zhang, X. Zhang, H. Liu, J. Li, Y. Chen, H. Duan, *Adv. Energy Mater.* **2021**, *11*, 2003927.
[66] Y. Zhang, G. Wang, F. Yu, G. Xu, Z. Li, M. Zhu, Z. Yue, M. Wu, H.-K. Liu, S.-X. Dou, C. Wu, *Chem. Eng. J.* **2021**, *416*, 128062.
[67] M. Wu, Y. Zhang, L. Xu, C. Yang, M. Hong, M. Cui, B. C. Clifford, S. He, S. Jing, Y. Yao, L. Hu, *Matter* **2022**, *5*, 3402.
[68] W. Sun, F. Wang, S. Hou, C. Yang, X. Fan, Z. Ma, T. Gao, F. Han, R. Hu, M. Zhu, C. Wang, *J. Am. Chem. Soc.* **2017**, *139*, 9775.
[69] X. Wang, Y. Li, *J. Am. Chem. Soc.* **2002**, *124*, 2880.

© 2023 The Authors. Advanced Functional Materials published by Wiley-VCH GmbH

16163028, 2023, 27, Downloaded from https://advanced.onlinelibrary.wiley.com/doi/10.1002/adfm.202302098, Wiley Online Library on [03/12/2025]. See the Terms and Conditions (https://onlinelibrary.wiley.com/terms-and-conditions) on Wiley Online Library for rules of use; OA articles are governed by the applicable Creative Commons License